The Astrophysical Journal Letters, 806:L16 (6pp), 2015 June 10 doi:10.1088/2041-8205/806/1/L16

NUCLEOSYNTHESIS IN A PRIMORDIAL SUPERNOVA: CARBON AND OXYGEN ABUNDANCES IN SMSS J031300.36–670839.3*

Michael S. Bessell[1], Remo Collet[1], Stefan C. Keller[1,9], Anna Frebel[2], Alexander Heger[3,10,11], Andrew R. Casey[4], Thomas Masseron[4], Martin Asplund[1], Heather R. Jacobson[5], Karin Lind[6], Anna F. Marino[1], John E. Norris[1], David Yong[1], Gary Da Costa[1], Conrad Chan[3], Zazralt Magic[7], Brian Schmidt[1], and Patrick Tisserand[8,12]
[1] Research School of Astronomy and Astrophysics, CPMS, The Australian National University, Canberra, ACT 2611, Australia; michael.bessell@anu.edu.au, remo.collet@anu.edu.au, stefan.keller@defence.gov.au, martin.asplund@anu.edu.au, anna.marino@anu.edu.au, john.norris@anu.edu.au, david.yong@anu.edu.au, gary.dacosta@anu.edu.au, brian.schmidt@anu.edu.au
[2] Department of Physics and Kavli Institute for Astrophysics and Space Science, Massachusetts Institute of Technology, Cambridge, MA 02139, USA; afrebel@mit.edu
[3] School of Physics and Astronomy, Monash University, VIC 3800, Australia; alexander.heger@monash.edu, conrad.chan@monash.edu
[4] Institute of Astronomy, University of Cambridge, Cambridge CB3 0HA, UK; arc@ast.cam.ac.uk, tpm40@ast.cam.ac.uk
[5] Kavli Institute for Astrophysics and Space Science, Massachusetts Institute of Technology, Cambridge, MA 02139, USA; hrj@mit.edu
[6] Department of Physics and Astronomy, Uppsala University, Box 516, SE-751 20, Uppsala, Sweden; karin.lind@physics.uu.se
[7] Max-Planck-Institut für Astrophysik, D-85741 Garching, Germany; magic@MPA-Garching.MPG.DE
[8] Sorbonne Universités, UPMC Univ Paris 06, UMR 7095, Institut d'Astrophysique de Paris, F-75014 Paris, France; tisserand@iap.fr
[9] Department of Defense, Australian Government, Canberra, ACT 2610, Australia
[10] School of Physics and Astronomy, University of Minnesota, Minneapolis, MN 55455, USA
[11] CNA, Department of Physics and Astronomy, Shanghai Jiao-Tong University, Shanghai 200240, P. R. China
[12] UPMC-CNRS, UMR7095, Institut d'Astrophysique de Paris, F-75014 Paris, France
Received 2015 March 13; accepted 2015 May 12; published 2015 June 8

ABSTRACT

SMSS J031300.36–670839.3 (hereafter SM0313–6708) is a sub-giant halo star, with no detectable Fe lines and large overabundances of C and Mg relative to Ca. We obtained Very Large Telescope–Ultraviolet and Visual Echelle Spectrograph (UVES) spectra extending to 3060 Å showing strong OH A-X band lines enabling an oxygen abundance to be derived. The OH A-X band lines in SM0313–6708 are much stronger than the CH C-X band lines. Spectrum synthesis fits indicate an [O/C] ratio of 0.02 ± 0.175. Our high signal-to-noise ratio UVES data also enabled us to lower the Fe abundance limit to $[Fe/H]_{\langle 3D\rangle,NLTE} < -7.52$ (3σ). These data support our previous suggestion that the star formed from the iron-poor ejecta of a single massive star Population III supernova.

Key words: stars: Population III – supernovae: general – supernovae: individual (SMSS J031300.36)

1. INTRODUCTION

Keller et al. (2014) described the discovery of SMSS J031300.36–670839.3 (hereafter SM0313–6708) and the analysis of the high resolution spectrum taken with the *Magellan* Inamori Kyocera Echelle (MIKE; Bernstein et al. 2003) spectrograph on the 6.5 m *Magellan* Telescope at Las Campanas Observatory in Chile. The spectrum was remarkable for the complete absence of lines of iron or any other metal, apart from Mg I and Ca II. The fact that no iron line is evident in the signal-to-noise ratio (S/N) ~ 100 (at $\lambda = 4000$ Å) spectrum indicated that the iron abundance in SM0313–6708 was at most [Fe/H] = −7.2,[13] making this star at least ~40 times more iron-poor than HE 1327–2326 ([Fe/H] = −5.6; Frebel et al. 2005).

The only elements whose abundances could be measured were lithium, carbon, magnesium, and calcium with $A(Li) = 12 + \log(Li/H) = 0.71 \pm 0.10$, [C/H] = −2.44 ± 0.10, [Mg/H] = −4.30 ± 0.10, and [Ca/H] = −7.2 ± 0.10, respectively. The level of lithium is presumably related to the decline from the primordial Spite plateau level of $A(Li) = 2.2$ during early post-main-sequence stellar evolution (Lind et al. 2009) and this evidence, together with a $T_{eff} = 5125$ K and $\log g = 2.3$ derived from spectrophotometry, is consistent with a star ascending the giant branch for the first time. The C, Mg, and Ca abundances can be attributed to a low energy Pop III SNe, and measurement of the oxygen abundance, in particular, offers an important test of this scenario. To measure the oxygen abundance in ultra-metal-poor K stars, however, it is necessary to work in the ultraviolet and observe the OH lines that persist well after the [O I] 6300.3 Å line has become undetectable.

2. OBSERVATIONS

In order to measure the OH (and CH) lines between 3100 and 3200 Å and obtain better detection limits on N, Na, V, Co, Ni, Fe, and Cu, we used Ultraviolet and Visual Echelle Spectrograph (UVES; Dekker et al. 2000) on the VLT (ESO Very Large Telescope) at Paranal in Chile. Between 2013 and 2014 September, 31 exposures totalling 29.26 hr of on-source integration were obtained. The UVES UV spectrum extended from 3060 to 3860 Å and the two red spectra from 4786 to 6803 Å.

The data were reduced using the default settings of the UVES pipeline as implemented in the "reflex" reduction environment. There was a high order sinusoidal-like modulation of the continuum remaining in much of the UV spectrum. The modulation with an amplitude of about 20% and frequency about 50 Å was removed by hand, leaving a residual variation of amplitude of 2%–4% and spacing of about 1.5 Å that makes the measurement of shallow features somewhat uncertain. It was very clear, however, that there were many strong OH lines present between the observational cutoff around 3060 and

* Based on observations obtained with European Southern Observatory (ESO) telescopes (proposal 092.D-0742).
[13] Logarithm of abundance ratio relative to present day solar surface abundances, $[A/B] = \log(n_A/n_B) - \log(n_A/n_B)_\odot$.

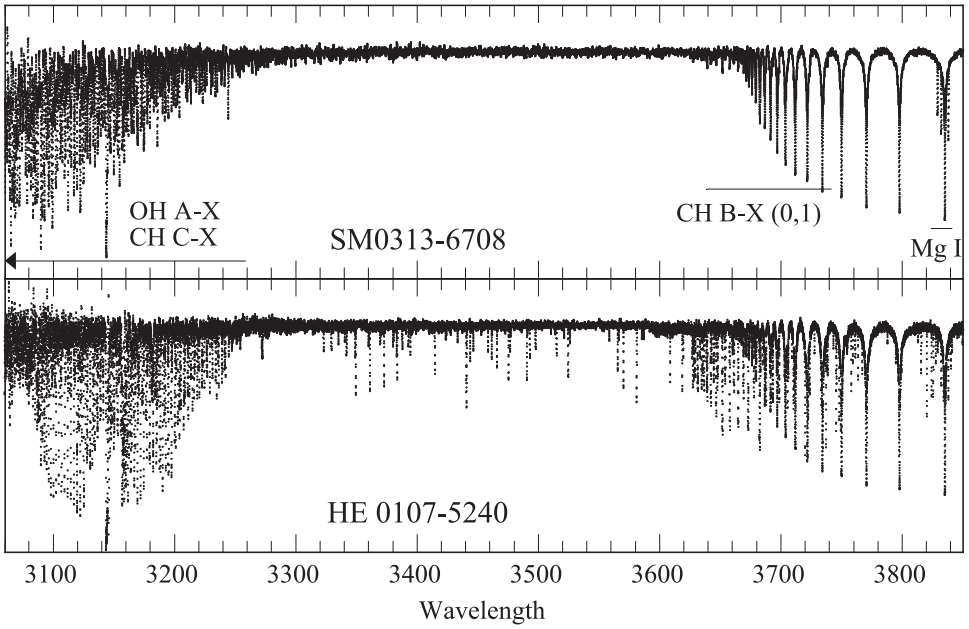

Figure 1. Normalized UVES UV spectra of SM0313–6708 and HE 0107–5240. Note the different distribution of the OH and CH lines in the two stars and the complete absence of metal lines in SM0313–6708 except for the similar strength Mg I lines.

3200 Å, and that the OH lines were much stronger than the CH lines, except at the band head of the CH C-X band near 3144 Å. In Figure 1 we compare the UV spectra of SM0313–6708 ([Fe/H] $\leqslant -7.2$) and HE 0107–5240 ([Fe/H] $= -5.4$), a C-rich ultra-EMP star with almost identical effective temperature and gravity, and possibly at the same evolutionary stage. The total absence of metal lines in SM0313–6708 (except for the Mg I lines around 3830 Å) is very marked as is the different distribution of the forest of molecular lines below 3250 Å. The CH lines dominate the spectrum of HE 0107–5240 whereas OH lines dominate in SM0313–6708. The complete absence of absorption lines in SM0313–6708 between 3250 and 3800 Å enables more stringent limits to be placed on those species with strong lines in that region.

3. ANALYSIS

We have carried out a spectrum synthesis of the CH, OH, and NH molecular lines in SM0313–6708 using Turbospectrum (Alvarez & Plez 1998; Plez 2012). We adopted an interpolated "standard" metallicity MARCS 1D LTE model atmosphere structure (Gustafsson et al. 2008), for $T_{\rm eff} = 5125$ K, log $g = 2.30$, [M/H] $= -5.0$, but with actual abundances from this paper for the atomic and molecular equilibria calculations. We used the new ^{12}CH and ^{13}CH line list from Masseron et al. (2014), while for OH and NH we used extensive line lists recently recomputed by T. Masseron (2015, in preparation). The Masseron OH gf values are very similar to those of Gillis et al. (2001), but the NH gf values are significantly smaller by 0.3 − 0.7 dex than the commonly used values of Kurucz (2011). The solar composition was adopted from Asplund et al. (2009).

We refitted the CH A-X and B-X lines in the blue MIKE spectrum and determined a carbon abundance of [C/H] $= -2.41 \pm 0.05$, very similar to the previously determined A-X value. The CH C-X band synthesis is in good agreement with the A-X and B-X bands. The synthesized spectrum well reproduces the observed CH lines in strength and position for all J values and for all branches observed.

The OH lines extend from 3060 to redward of 3200 Å. Because of the lower S/N and the uncertain continuum placement at the shortest wavelengths where the lines are strongest, we derived the oxygen abundance in SM0313–6708 by fitting the weaker OH lines between 3178 and 3200 Å. Figure 2 clearly shows that the oxygen abundance is well constrained at [O/H] $= -2.00 \pm 0.10$. In HE 0107–5240, the similar temperature and gravity star with abundances [M/H] ≈ -5.4, [C/H] $= -1.58$ (Christlieb et al. 2004) and [O/H] $= -3.0$ (Bessell et al. 2004), these longer wavelength regions could not be used for OH fitting as they are dominated by CH lines as seen in Figure 3. We note that the treatment of scattering (as done in Turbospectrum), is very important for the analysis of the UV lines in SM0313–6708 and metal-poor giants in general.

Figure 3 shows the comparison between the observed and synthetic spectra at the shorter wavelengths in SM0313–6708 and HE 0107–5240. The panels on the left show the region that was used to measure the oxygen abundance in HE 0107–5240, and the panels on the right shows the region around the CH C-X band head. Note the significantly different relative strengths of OH and CH lines in the two stars.

There is no indication of any NH features centered on 3360 Å, but the higher S/N of the UVES spectrum enables us to reduce the upper limit to [N/H] $<-$ 4.2, at least two orders of magnitude lower than C and O.

3.1. 3D–1D Corrections to C and O Abundances

The carbon, nitrogen, and oxygen abundances reported above were derived from 1D LTE analysis of the CH and OH lines. One of us (RC) generated a 3D time-dependent hydrodynamic model atmosphere of a red giant star with stellar parameters very similar to the ones of SM0313–6708 using a custom version of the Stagger code (Nordlund & Galsgaard 1995; Nordlund et al. 2009) as well as a 1D model

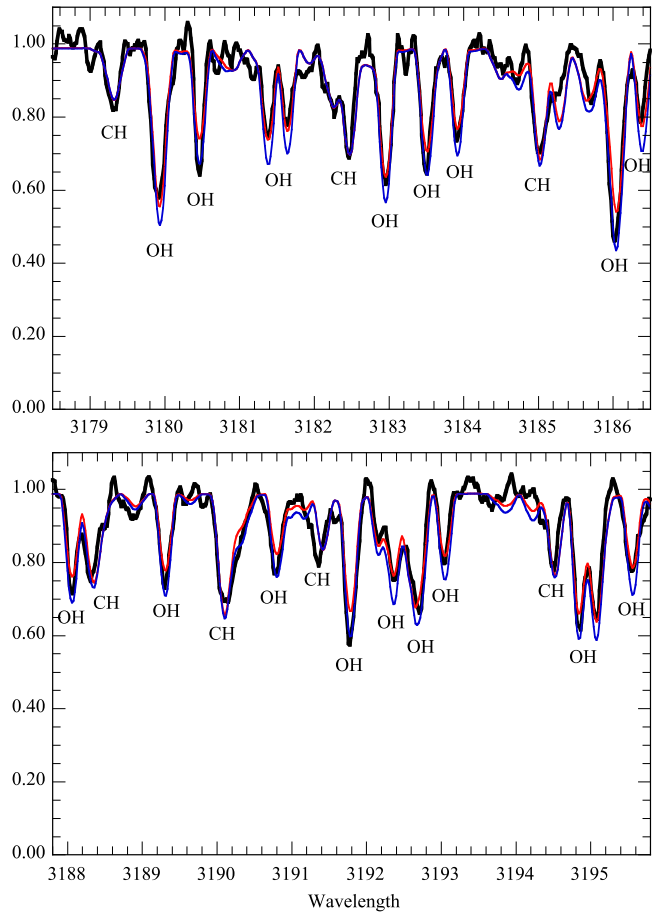

Figure 2. Region between 3178 and 3196 Å in SM0313–6708. Observations (thick black line); synthetic spectra for [C/H] = −2.41 and oxygen abundance [O/H] = −2.10 (red line) and higher abundance [O/H] = −1.90 (blue line). Although the OH lines here are weaker than the 3060–3200 Å region, the S/N is higher and the continuum level is better defined.

atmosphere corresponding to the same parameters and relying on the same microphysics and opacity data. Synthetic LTE CH and OH spectra for a range of C and O abundances were produced using the SCATE code (Hayek et al. 2011) with 3D and 1D models, accounting for the effects of radiative scattering; the best fits to the observed spectrum were determined in both cases and the 3D–1D abundance corrections were then derived. These 3D–1D corrections are: −0.14 dex for the carbon abundance as derived from the CH band and −0.53 dex for oxygen from OH (the negative sign meaning the 3D-derived abundances are lower). The 3D-corrected [O/C] ratio in SM0313–6708 is therefore +0.02 with an uncertainty of 0.175 dex. A 3D–1D correction of −0.50 dex to the 1D nitrogen abundance was also derived with similar 3D and 1D LTE calculations but based purely on the comparison of synthetic 3D and 1D spectra.

The poorer fit of the deep OH and CH lines in Figure 3 is likely due to limitations with the adopted 1D model atmosphere. Our computations of CH, NH, and OH lines have been carried out in LTE, but in low-density atmospheres it is possible that non-LTE processes may be important for cooling the outer stellar layers (Lambert et al. 2013) and for affecting the strength of molecular bands. As no study of non-LTE CH, NH, and OH line formation is available in the literature, however, we are unable to quantify non-LTE effects on CNO abundances derived from these molecular bands.

3.2. $^{12}C/^{13}C$ Ratio

In order to put limits on the $^{12}C/^{13}C$ ratio we used two regions of the spectrum where the ^{12}CH and ^{13}CH lines are well separated and free from blending. There were five strong lines in the B-X region and nine in the A-X region. Sections of spectrum centered on each of the lines were extracted and summed in both the observed spectrum and the synthetic spectra. The summed observed and synthetic ^{12}CH lines were in good agreement, but no ^{13}CH feature was evident in the summed spectrum. This allows us to place a three sigma lower limit of about 40 for the $^{12}C/^{13}C$ ratio. This low value of ^{13}C is consistent with massive Population III star yields with no or little primary nitrogen production (Heger & Woosley 2010).

3.3. Revised Upper Limits on the Abundances of Fe, Na, Si, Sc, V, Co, Ni, Cu

Two of the Fe I transitions with the largest log *gf* values in the observed spectral range are located within the highest S/N portion of the UV spectrum, at 3719.94 and 3737.13 Å. Sections around the position of these lines were extracted, summed and compared with the summed synthetic spectra computed for a range of Fe abundances. Again, no feature was evident in the observed spectrum, and we estimate a revised abundance limit for [Fe/H] of about −7.5.

The non-detection of lines of Sc, Ti, V, Co, Ni, and Cu in the UVES spectrum in the range from 3100 to 3700 Å provided revised lower upper limits for many elements given in Table 1 (A. Frebel et al. 2015, in preparation). The non-detection of the Si I line at 3905.52 Å in the blue MIKE spectrum indicates an upper limit of −5.6 dex.

The UVES red spectrum was in good agreement with the MIKE spectrum for the Mg I lines and the Li I line, but the better S/N and weaker telluric lines in the UVES red spectrum indicates that the Na limit could be lowered to about −5.7 dex. Table 1 lists the current best estimates for the chemical abundances of SM0313–6708.

4. DISCUSSION

Heger & Woosley (2010) have followed the evolution and explosion of metal-free stars with masses 10 $M_\odot$–100 $M_\odot$ and determined their nucleosynthetic yields, light curves, and remnant masses. Such stars would have been the first to form after the Big Bang and could have left a distinctive imprint on the composition of the early universe. The evolution of these stars may be affected in several ways by their zero-metallicity primordial composition. Because these stars suffered little mass-loss during their pre-explosive lifetimes, their masses at their deaths were larger than more metal-rich stars. The models produces some carbon, but for masses less than about 40 $M_\odot$ primary production of nitrogen is suppressed. These stars ended their lives as compact blue supergiants making their envelope more tightly bound, with two interesting consequences: (i) the more compact envelope increases the amount of mass that falls back after the explosion, meaning that they were more likely to collapse to black holes at lower masses compared to modern stars, trapping most of the heavy elements; (ii) mixing by the Rayleigh–Taylor instabilities is suppressed in these compact stars, so it is mainly unmixed

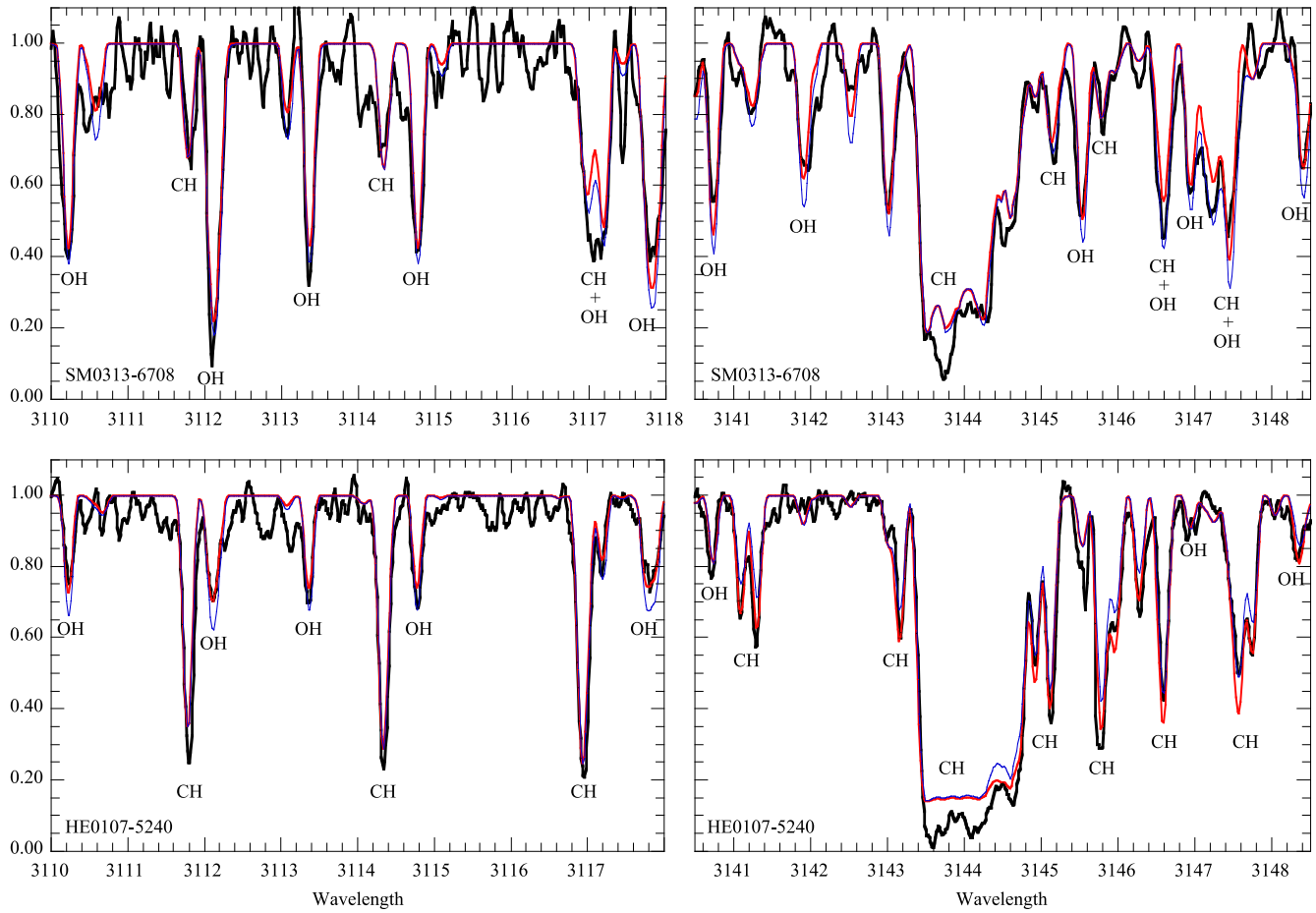

Figure 3. Spectral region showing mainly OH lines (left) and a region around the CH C-X band head (right). Top: SM0313–6708. Observations (thick black line); synthetic spectra for abundance [O/H] = −2.10 (red line) and higher abundance [O/H] = −1.90 (blue line). [C/H] = −2.41 in both syntheses. The 3110–3118 Å region has low S/N and uncertain continuum placement. Bottom: HE 0107–5240. Observations (thick black line). Left: synthetic spectra for best-fitting abundances [C/H] = −1.20, [O/H] = −2.55 (red line) and higher abundance [O/H] = −2.40 (blue line). Right: [O/H] = −2.55, [C/H] = −1.20 (red line) and lower abundance [C/H] = −1.40 (blue line).

material that escapes in the explosion. Heger & Woosley (2010) fitted their predicted nucleosynthetic yields to several examples of metal-poor stars and found that the best fits were obtained from relatively low energy explosions of 0.6–1.8 B (1 B = 10^{51} erg) as compared to hypernova models (Nakamura et al. 2001). Overall, the large sample of metal-poor stars in Cayrel (2004) was well fit with a normal Salpeter IMF including all stars from 10 $M_{\odot}$ to 100 $M_{\odot}$ (but with a preference for stars lighter than 15 $M_{\odot}$), a small amount of fallback and with reduced mixing of 1% of the helium core mass (for reference, the default mixing value adopted to solar metallicity stars is 10% of the helium core mass; Heger & Woosley 2010). For the two ultra-iron-poor, but high O/Fe, stars HE 0107–5240 (Bessell et al. 2004; Christlieb et al. 2004) and HE 1327–2326 (Aoki et al. 2006; Frebel et al. 2006), the best fits were for similar low energy explosions, a lower upper mass range (10 $M_{\odot}$ to less than 30 $M_{\odot}$), small fallback and an even lower mixing of 0.025.

The abundances of SM0313–6708 are much more extreme than the Cayrel (2004) EMP stars or the two C-rich ultra-EMP stars. The biggest difference are the large carbon, oxygen and magnesium overabundances relative to calcium, and the non-detection of all other metals. Of particular significance is the oxygen to carbon ratio in SM0313–6708 of $[O/C]_{3D} = +0.02$ compared to $[O/C]_{3D} \approx -1.0$ (Collet et al. 2006) in HE 0107–5240.

Fitting the current SM0313–6708 abundances (Table 1) against models from Heger & Woosley (2010) using their Starfit algorithm[14] finds good fits for progenitor masses in the range 40 $M_{\odot}$ − 60 $M_{\odot}$ and energies of 1.5 B − 1.8 B with low amounts of mixing, $\lesssim$2%. This low amount of mixing is consistent with Heger & Woosley (2010) and hydrodynamic models of Pop III SNe by Joggerst et al. (2009). The best matching mass is sensitive to the upper limits of the Na and Al abundances. Generally, lower values on the upper limits to the abundances would push the fit toward higher initial masses, stars that produce a stronger odd–even effect. The low limits on N in SM0313–6708 constrain the mass on the upper end.

The range of [O/C] abundances produced in a range of core collapse supernovae is shown in Figure 4 together with a 40 $M_{\odot}$ fit from Starfit. Significantly, the observed [O/C] ratio is lower than what Pop III pair-instability SNe of Heger & Woosley (2002) can produce or what we can produce for high explosion energies ($E \gtrsim 3$ B) in more massive stars ($M \gtrsim 20\ M_{\odot}$). The structure and pre-SN evolution of stars with mass above 15 $M_{\odot}$ is very sensitive to initial mass (e.g., Sukhbold & Woosley 2014) and these stars may experience

[14] See also http://starfit.org (C. Chan et al. 2015, in preparation).

Table 1
Chemical Abundances of SM0313–6708

Element	$[X/H]_{1D,LTE}$	$[X/H]_{1D,NLTE}$	$[X/H]_{\langle 3D\rangle,LTE}$	$[X/H]_{\langle 3D\rangle,NLTE}$	$[X/H]_{3D,LTE}$
Li I[a]	0.70 ± 0.10	0.73 ± 0.10	…	0.56 ± 0.10	0.71 ± 0.10
C (CH)[b]	−2.41 ± 0.05	…	…	…	−2.55 ± 0.09
N (NH)[b]	<−4.2	…	…	…	<−4.70
O (OH)[b]	−2.00 ± 0.10	…	…	…	−2.53 ± 0.15
Na I[b]	<−5.7	<−5.65	<−5.79	<−5.66	…
Mg I[b]	−4.45 ± 0.07	−4.03 ± 0.03	−4.53 ± 0.09	−4.08 ± 0.03	…
Al I[b]	<−6.2	…	…	…	…
Si I[b]	<−5.6	…	…	…	…
Ca II	−7.46 ± 0.10	−7.27 ± 0.10	−7.60 ± 0.10	−7.26 ± 0.10	…
Sc II[b]	<−5.5	…	…	…	…
Ti II[b]	<−7.1	…	…	…	…
V II[b]	<−4.3	…	…	…	…
Cr I	<−6.3	…	…	…	…
Mn I	<−5.8	…	…	…	…
Fe I[b]	<−7.80	<−7.28	<−8.27	<−7.52	…
Co I[b]	<−5.4	…	…	…	…
Ni I	<−6.9	…	…	…	…
Cu I[b]	<−5.5	…	…	…	…
Zn I	<−3.4	…	…	…	…
Sr II	<−6.9	…	…	…	…
Ba II	<−6.1	…	…	…	…
Eu II	<−2.9	…	…	…	…

Notes. Estimated (1σ) observational uncertainties in the quoted upper limit abundances are 0.3 dex. For Fe the uncertainty is 3σ. Bold print indicates our *recommended* values used in the fitting of explosive nucleosynthesis.
[a] The abundance of Li is expressed as $A(\mathrm{Li}) = \log(\mathrm{N(Li)/N(H)}) + 12$.
[b] Abundances derived in this paper.

chaotic nuclear burning. As a result, the fraction of the C and O layers that are ejected varies strongly for a given explosion energy and is rather sensitive to mass and explosion energy. Currently there is no good first principle calculations providing reliable predictions for explosion energies for a given stellar structure for masses above 15 $M_{\odot}$.

Our new 3D LTE values provide definite constraints on the [O/C] ratio instead of only an upper limit. The new lower value of [Fe/H] derived here strengthens the constraint *not* to eject iron group elements from the inner core of the progenitor star. This limits the explosion energy and the magnitude of mixing due to Raleigh–Taylor instabilities during the SN explosion.

Ishigaki et al. (2014) have proposed an alternative scenario to explain the unique abundances in SM0313–6708. They investigated supernova yields of metal-free (Population III) stars and find that the high [C/Ca] and [C/Mg] ratios and upper limits of other elemental abundances are well reproduced with the yields of core-collapse supernovae (which have normal kinetic energies of explosion of 1 B) and hypernovae (10 B) of Population III 25 $M_{\odot}$ or 40 $M_{\odot}$ stars. Their best-fit models assume that the explosions undergo extensive matter mixing and fallback, leaving behind a black hole remnant. In these models, Ca is produced by static/explosive O burning and incomplete Si burning in the Population III supernova/hypernova, in contrast to our suggestion that the Ca originates from the hot-CNO cycle during pre-supernova evolution, which is, remarkably, consistent with the present data.

Although Ishigaki et al. (2014) well fits the observed abundances, their modeling uses several independent free parameters. For example, their models require significantly more mixing than is consistent with hydrodynamical simulations of Population III stars (Joggerst et al. 2009) and the fallback is adjusted independently of the explosion energy. Jetted or asymmetric explosions may be a possibility; however, this is another free parameter. In the Heger & Woosley (2010) models the mixing is consistent with hydrodynamical simulations of Joggerst et al. (2009) and the fallback is computed self-consistently with the explosion energy. Fuller discussion of the abundances of SM0313–6708 and SN modeling will be presented in a future paper.

5. CONCLUSIONS

The ultraviolet spectrum of SM0313–6708 is dominated by the lines of the OH A-X band, which are noticeably stronger than the CH C-X lines. The new line lists of Masseron fit the OH and CH lines very well in both wavelength and strength. We could detect no lines of ^{13}CH, which places a limit of more than 40 on $^{12}C/^{13}C$, and no lines of NH putting nitrogen at least two orders of magnitude less than C and O. This supports there having been no mixing from the H-burning shell to the surface within SM0313–6708 and there being little nitrogen relative to C and O in the material from which SM0313–6708 formed. The clear lack of any metal lines apart from Mg I in the UVES ultraviolet spectrum also enabled us to lower the abundance limits for those elements whose strong lines are normally seen in this region, including Fe I, for which we now derive an [Fe/H] upper limit of −7.52 dex (3σ) from $\langle 3D\rangle$ LTE analysis. We derived an [O/C] ratio of +0.02 with a 1σ uncertainty of 0.175 dex for SM0313–6708, updated abundances measurements for Mg and Ca, and derived new upper limits for nitrogen, the Fe-group elements and some of the alpha-elements. These abundances remain consistent with a single massive Population III progenitor in the mass range

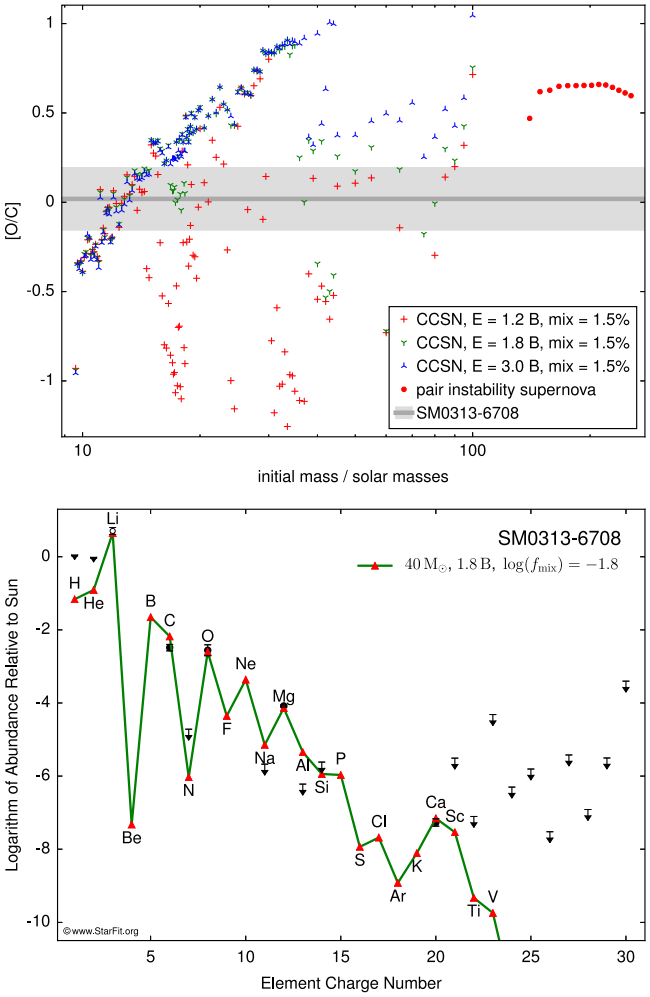

Figure 4. Top: range of [O/C] abundances produced in a range of core collapse supernovae for three different explosion energies, 1.2 B, 1.8 B, and 3 B and mixing of 1.5% (of helium core size; see Heger & Woosley 2010). The dark gray line and the light gray shading show the derived SM0313–6708 and its 1σ error bar of 0.175 dex. Red dots show the [O/C] ratios for Pop III pair-instability supernovae (Heger & Woosley 2002). Bottom: the yields from stars in the $40\,M_{\odot}$–$60\,M_{\odot}$ range provide the best fit to the observed abundance pattern of all the elements (see the main text). The $40\,M_{\odot}$ fit is shown here.

$40\,M_{\odot}$–$60\,M_{\odot}$, low mixing, and modest explosion energies; the Ca production remains consistent with an origin from hydrostatic hydrogen burning. Improved upper limits on intermediate-mass elements, in particular Na and Al, will further help constrain the models in the future. The strong Fe II lines in the vacuum UV between 2340 and 2625 Å should allow one to constrain—or detect—the iron abundance of SM0313–6708 down to as low as [Fe/H] = −9.

A.H. was supported by an Australian Research Council (ARC) Future Fellowship (FT120100363). R.C. is supported by an ARC Discovery Early Career Researcher Award (DE120102940). A.C. and T.M. have been supported by the European Union FP7 programme through ERC grant number 320360. A.F. acknowledges support from NSF Career grant AST-1255160. This research been supported, in part, by ARC Discovery Project grants DP120101237 and DP150103294 and NSF grant PHY-1430152 (JINA-CEE).

Facility: ESO(UVES)

REFERENCES

Aoki, W., Frebel, A., Christlieb, N., et al. 2006, ApJ, 639, 897
Alvarez, R., & Plez, B. 1998, A&A, 330, 1109
Asplund, M., Grevesse, N., Sauval, A. J., & Scott, P. 2009, ARA&A, 47, 481
Bernstein, R., Shectman, S. A., Gunxnels, S. M., Mochnacki, S., & Athey, A. E. 2003, Proc. SPIE, 4841, 1694
Bessell, M. S., Christlieb, N., & Gustafsson, B. 2004, ApJL, 612, L61
Cayrel, R., et al. 2004, A&A, 416, 1117
Christlieb, N., Gustafsson, B., Korn, A. J., et al. 2004, ApJ, 603, 708
Collet, R., Asplund, M., & Trampedach, R. 2006, ApJ, 644, 121
Dekker, H., D'Odorico, S., Kaufer, A., Delabre, B., & Kotzlowski, H. 2000, Proc. SPIE, 4008, 534
Frebel, A., Aoki, W., Christlieb, N., et al. 2005, Natur, 434, 871
Frebel, A., Christlieb, N., Norris, J. E., Aoki, W., & Asplund, M. 2006, ApJL, 638, L17
Gillis, J. R., Goldman, A., Stark, G., & Rinsland, C. P. 2001, JQSRT, 68, 225
Gustafsson, B., Edvardsson, B., Eriksson, K., et al. 2008, A&A, 486, 951
Hayek, W., Asplund, M., Collet, R., & Nordlund, Å. 2011, A&A, 529, A158
Heger, A., & Woosley, S. E. 2002, ApJ, 567, 532
Heger, A., & Woosley, S. E. 2010, ApJ, 724, 341
Ishigaki, M. N., Tominaga, N., Kobayashi, C., & Nomoto, K. 2014, ApJL, 792, L32
Joggerst, C. C., Woosley, S. E., & Heger, A. 2009, ApJ, 693, 1780
Keller, S. C., Bessell, M. S., Frebel, A., et al. 2014, Natur, 506, 463
Kurucz, R. 2011, http://kurucz.harvard.edu/linelists/linesmol/nh.asc
Lambert, J., Josselin, E., Ryde, N., & Faure, A. 2013, in Betelgeuse Workshop,, ed. P. Kervella, T. Le Bertre, & G. Perrin (EAS Publication Series, Vol. 60; Les Ulis, France: EDP Sciences), 111
Lind, K., Primas, F., Charbonnel, C., Grundahl, F., & Asplund, M. 2009, A&A, 503, 545
Masseron, T., Plez, B., van Eck, S., et al. 2014, A&A, 571, 47
Nakamura, T., Umeda, H., Iwamoto, K., et al. 2001, ApJ, 555, 880
Nordlund, Å., & Galsgaard, K. 1995, in A 3D MHD Code for Parallel Computers, Tech. Rep. (Copenhagen: Niels Bohr Institute), http://www.astro.ku.dk/kg/Papers/MHD_code.ps.gz.
Nordlund, Å., Stein, R. F., & Asplund, M. 2009, LRSP, 6, 2
Plez, B. 2012, Turbospectrum: Code for Spectral Synthesis, Astrophysics Source Code Library, record ascl:1205.004
Sukhbold, T., & Woosley, S. E. 2014, ApJ, 783, 10